GLIAL CELL SIGNALING

Circuit-specific signaling in astrocyte-neuron networks in basal ganglia pathways

R. Martín,[1*] R. Bajo-Grañeras,[1*] R. Moratalla,[1,2] G. Perea,[1] A. Araque[3]†

Astrocytes are important regulatory elements in brain function. They respond to neurotransmitters and release gliotransmitters that modulate synaptic transmission. However, the cell- and synapse-specificity of the functional relationship between astrocytes and neurons in certain brain circuits remains unknown. In the dorsal striatum, which mainly comprises two intermingled subtypes (striatonigral and striatopallidal) of medium spiny neurons (MSNs) and synapses belonging to two neural circuits (the direct and indirect pathways of the basal ganglia), subpopulations of astrocytes selectively responded to specific MSN subtype activity. These subpopulations of astrocytes released glutamate that selectively activated *N*-methyl-D-aspartate receptors in homotypic, but not heterotypic, MSNs. Likewise, astrocyte subpopulations selectively regulated homotypic synapses through metabotropic glutamate receptor activation. Therefore, bidirectional astrocyte-neuron signaling selectively occurs between specific subpopulations of astrocytes, neurons, and synapses.

Astrocytes respond to synaptically released neurotransmitters and release gliotransmitters that regulate synaptic transmission [(*1*–*6*), but see (*7*–*8*)]. However, the question of whether this functional relationship is cell- and synapse-specific remains unexplored. To address this issue, we studied the dorsal striatum, which presents unique structural and functional properties, because it mainly comprises two subtypes of intermingled but molecularly identifiable neurons [striatonigral and striatopallidal medium spiny neurons (MSNs)] and synapses belonging to two distinct neural circuits (the basal ganglia's direct and indirect pathways). Hence, individual MSNs can be selectively stimulated while analyzing the astrocytic activity and the consequent neuromodulation of particular neurons and synapses.

We first performed paired recordings of MSNs, stimulating one neuron by depolarization and monitoring corticostriatal excitatory postsynaptic currents (EPSCs) in that neuron (homoneuronal synapses) as well as in the adjacent neuron (heteroneuronal synapses) (Fig. 1A and supplementary materials). The stimulation of single MSNs by depolarizing pulses or action potential trains (fig. S1), which trigger endocannabinoid (eCB) release (*9*–*12*), induced a transient depression (76.5 ± 2.9% relative to the control EPSC amplitude, $P < 0.001$) in 16 out of 33 homoneuronal synapses (48.5%) (Fig. 1, B and C). This synaptic depression was abolished by the cannabinoid receptor type 1 (CB1R) antagonist AM251 (2 μM, n = 10 MSN pairs), was absent in slices from CB1R-deficient ($CB1R^{-/-}$) mice (n = 24 MSN pairs) (Fig. 1C), and was associated with an increase in the paired-pulse ratio (PPR; n = 16 MSN pairs) (fig. S1G). This indicates that the depression corresponded to a depolarization-induced suppression of excitation (DSE) mediated by the activation of presynaptic CB1Rs (*13*).

In contrast, in simultaneously recorded heteroneuronal synapses, MSN stimulation induced a transient potentiation (138.5 ± 7.7% relative to the control EPSC amplitude, $P < 0.001$) in 7 out of 16 synapses (43.8%) (Fig. 1, B and C) that concomitantly evoked DSE in homoneuronal synapses. No changes were detected in the rest of the heteroneuronal synapses (fig. S2). This potentiation was abolished by AM251 (n = 7 MSN pairs), was absent in $CB1R^{-/-}$ mice (n = 24) (Fig. 1C), and was accompanied by a PPR decrease (n = 7 MSN pairs) (fig. S1G), indicating that it was also mediated by CB1R activation. Because the eCB-mediated DSE has been well characterized in MSNs (*9*, *12*), we focused our study on the heteroneuronal synaptic responses.

The two types of MSNs are not spatially segregated, but they express different dopamine receptors. Their projections form the origin of the direct and indirect pathways of the basal ganglia motor circuit. Direct-pathway striatonigral MSNs express D1 receptors, and indirect-pathway striatopallidal MSNs express D2 receptors (termed D1 and D2 MSNs, respectively) (*14*, *15*). We investigated whether eCB-mediated heteroneuronal synaptic potentiation was specific of the neuronal subtypes, using Drd1a-tdTomato and Drd2-EGFP bacterial artificial chromosome (BAC) transgenic mice that respectively allowed the identification of the D1 and D2 MSNs (*16*, *17*) (Fig. 1D). We recorded homotypic (D1-D1 or D2-D2) and heterotypic (D1-D2) pairs of MSNs, stimulating one neuron to evoke eCB release and analyzing synaptic transmission in the other neuron (Fig. 1E). Stimulation of either D1 or D2 MSNs induced a heteroneuronal potentiation selectively in homotypic pairs (n = 10 out of 11 D1-D1 pairs and 11 out of 12 D2-D2 pairs), but no synaptic changes were observed in heterotypic MSNs (n = 13 D1-D2 and 12 D2-D1 pairs in which D1 and D2 MSNs were stimulated, respectively) (Fig. 1F). This heteroneuronal potentiation between homotypic neurons was abolished by AM251 (n = 10 D1-D1 and 11 D2-D2 pairs) and absent in mice produced by crossing Drd1a-tdTomato and $CB1R^{-/-}$ mice (D1-Tom-$CB1R^{-/-}$; n = 13 D1-D1 and 12 nonfluorescence and putatively D2-D2 pairs) (Fig. 1G). The different synaptic regulation of homotypic and heterotypic neurons was not due to differences in eCB release, because only neuronal pairs that showed homoneuronal DSE were considered (fig. S3). Taken together, these results indicate cell-specific signaling between MSN subtypes belonging to the direct or indirect basal ganglia pathways.

The synaptic potentiation of homotypic MSNs was abolished by antagonists of the group I metabotropic glutamate receptors ($mGluR_{5/1}$) MPEP (50 μM) and LY367385 (100 μM), suggesting the participation of glutamate (n = 10 D1-D1 and 11 D2-D2 pairs) (Fig. 1G). Consistent with a presynaptic mechanism suggested by PPR changes, in paired recordings of homotypic MSNs in which one neuron was loaded with guanosine 5´-*O*-(2´-thiodiphosphate) (GDP-β-S; 2 mM) to prevent postsynaptic mGluR-mediated signaling (confirmed by the absence of calcium elevations in response to application of the $mGluR_{5/1}$ agonist DHPG) (Fig. 2, A to C), neuronal stimulation similarly evoked heteroneuronal potentiation, enhanced miniature EPSC (mEPSC) frequency but not amplitude, and decreased PPR in control and GDP-β-S–loaded neurons (Fig. 2, D to F). Moreover, local application of DHPG mimicked these responses (Fig. 2, D to F), further supporting an mGluR-dependent presynaptic mechanism.

The neuronal release of eCBs can activate astrocytic CB1Rs and stimulate glutamate release in the hippocampus and cortex (*18*–*20*). We thus tested whether astrocytes responded to eCBs released from MSNs by monitoring astrocyte Ca^{2+} levels in response to neuronal stimulation (Fig. 2, G and H, and fig. S4). MSN depolarization elevated Ca^{2+} in 71 out of 153 astrocytes (46.4% of astrocytes, 16 slices), increasing both the Ca^{2+}-spike probability and the oscillation frequency (Fig. 2, G to H). This astrocyte Ca^{2+} signal was abolished by AM251 and was absent in $CB1R^{-/-}$ and inositol 1,4,5-trisphosphate receptor type 2–deficient ($IP_3R2^{-/-}$) mice, in which heterotrimeric guanine nucleotide-binding protein (G protein)–mediated Ca^{2+} elevations are selectively impaired in astrocytes (*18*, *21*–*23*). Therefore, eCBs released from MSNs elevated astrocytic Ca^{2+} through CB1R activation (Fig. 2H).

We then tested whether the heteroneuronal potentiation required the astrocyte Ca^{2+} signal. This potentiation was absent in $IP_3R2^{-/-}$

[1]Instituto Cajal, Consejo Superior de Investigaciones Científicas, 28002 Madrid, Spain. [2]Centro de Investigación Biomédica en Red Enfermedades Neurodegenerativas, Instituto de Salud Carlos III, 28029 Madrid, Spain. [3]Department of Neuroscience, University of Minnesota, Minneapolis, MN 55455, USA.
*These authors contributed equally to this work.
†Corresponding author. E-mail: araque@umn.edu

mice (n = 28) (Fig. 2I); however, DSE recorded in homoneuronal synapses was unaffected (fig. S5) (*18*), indicating that the eCB-release machinery and neuronal CB1R activation was preserved in these animals. Conversely, the selective increase of Ca^{2+} levels by ultraviolet (UV)–flash photolysis of the Ca^{2+} cage *o*-nitrophenyl-EGTA (NP-EGTA), loaded in whole-cell recorded astrocytes, potentiated the synaptic transmission.

We next monitored *N*-methyl-D-aspartate receptor (NMDAR)–dependent neuronal slow inward currents (SICs) (*24*–*26*), which are a biological assay to detect astrocytic glutamate release (*1*). In MSN-pair recordings, stimulation of one neuron elevated astrocyte Ca^{2+} levels and increased the frequency of SICs in adjacent MSNs (Fig. 2; G, J, and K). SICs were abolished by the NMDAR antagonist AP5 (50 μM), without affecting the astrocyte Ca^{2+} signals (n = 11 MSN pairs), and were unaffected by tetrodotoxin (1 μM, n = 8 MSN pairs) (Fig. 2L). These results indicate that striatal astrocytes may release glutamate upon elevating their Ca^{2+} levels (fig. S6). Local application of the CB1R agonist WIN55,212-2 (WIN; 100 μM) mimicked the neuron-evoked increase of both astrocyte Ca^{2+} levels and SIC frequency (n = 15 MSNs) (fig. S7). Neuronal- and WIN-evoked Ca^{2+} elevations and SICs were abolished by AM251 and absent in $CB1R^{-/-}$ and $IP_3R2^{-/-}$ mice (Fig. 2H and fig. S7). Hence, eCBs released from MSNs activate CB1Rs in astrocytes, which elevate their intracellular Ca^{2+} and stimulate the release of glutamate that activates neuronal NMDARs. In aggregate, these findings indicate that MSNs signal to astrocytes through eCBs, and, in turn, astrocytes signal to MSNs through glutamate.

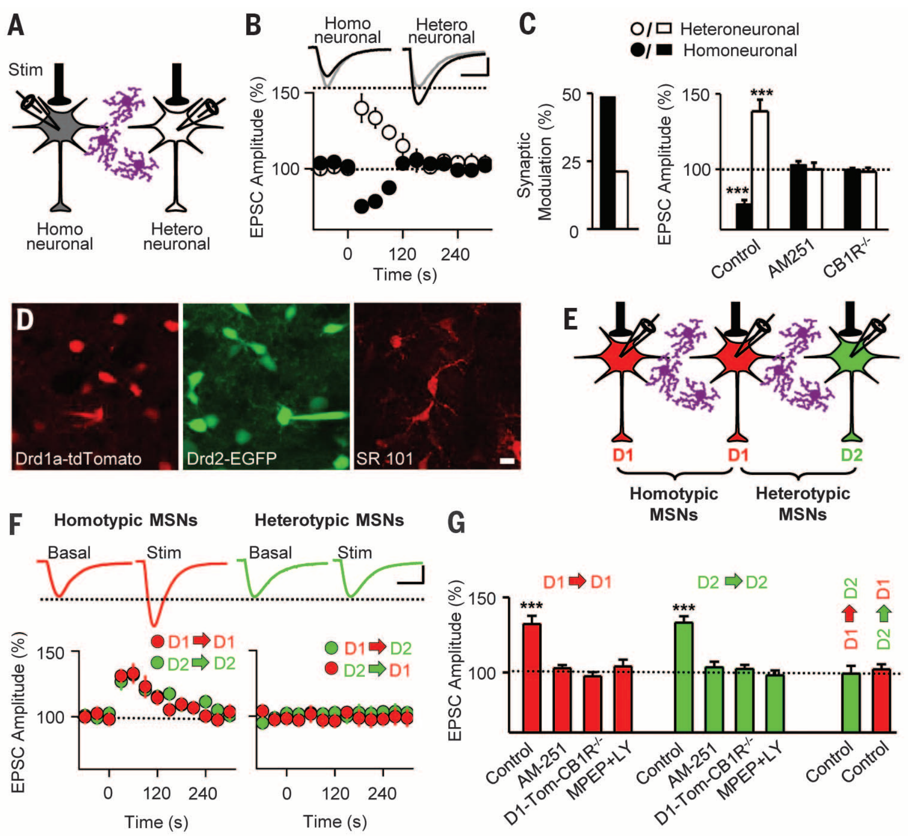

Fig. 1. Differential modulation of synaptic transmission by eCBs in the dorsal striatum. (**A**) Scheme showing depolarization of one MSN while EPSCs were monitored in that neuron (homoneuronal) and in the adjacent neuron (heteroneuronal). Astrocytes are shown in purple. (**B**) Representative EPSCs (top) before (gray) and after (black) neuronal stimulation, with relative responses (bottom) in homoneuronal (black circles) and heteroneuronal (white circles) synapses. On the x axis, 0 s corresponds to the onset of the neuronal stimulation, as in all other figures. The scale bars are 25 pA (vertical) and 10 ms (horizontal). (**C**) The percentage of homoneuronal and heteroneuronal synapses showing modulation (left) and relative EPSC amplitude in control, AM251, and $CB1R^{-/-}$ mice (each bar: $n \geq 7$ synapses, $n \geq 7$ slices) (right). (**D**) Fluorescence images of MSNs from Drd1a-tdTomato and Drd2-EGFP BAC-transgenic mice and sulforhodamine 101 (SR101)–stained astrocytes. The scale bar is 10 μm. (**E**) Scheme of our experimental paradigm. (**F**) Averaged EPSCs (top) before (basal) and after D1- or D2-MSN stimulation (stim) in homotypic and heterotypic MSNs, with EPSC amplitudes (bottom). The scale bars are 25 pA (vertical) and 15 ms (horizontal). (**G**) Relative EPSC amplitude changes in control, AM251, D1-Tom-$CB1R^{-/-}$ mice, and MPEP+LY367385 (MPEP+LY) (each bar: $n \geq 10$ MSNs, $n \geq 10$ slices). ***P < 0.001; Student´s t test. Data are expressed as mean ± SEM.

We then studied whether the reciprocal signaling between astrocytes and MSNs was cell type–specific and pathway-specific. First, we investigated whether subpopulations of astrocytes were functionally associated with MSN subtypes by monitoring astrocytic Ca^{2+} levels and recording pairs of identified homotypic or heterotypic MSNs. The number of responding astrocytes, as well as the increase in the Ca^{2+}-spike probability and oscillation frequency, were similar upon stimulation of D1 and D2 MSNs (Fig. 3, A to D). However, whereas 55.4 ± 7.0% (n = 117 astrocytes, 14 slices) and 46.1 ± 4.8% (n = 129 astrocytes, 12 slices) of the astrocytes responded to depolarization of homotypic D1-D1 or D2-D2 MSNs, respectively, only 10.7 ± 3.2% of the astrocytes (n = 118 astrocytes, 14 slices) responded to stimulation of both types of D1-D2 MSNs in heterotypic pairs (Fig. 3, E to G). Subsets of astrocytes thus selectively responded to the activity of either D1 or D2 MSNs, which suggests the existence of specific neuron-to-astrocyte signaling between specific MSN subtypes and particular striatal astrocytes.

We then tested whether the astrocyte-to-neuron signaling shown in Fig. 2 was restricted to particular neuronal subtypes by analyzing SICs in identified MSN pairs. In homotypic pairs, stimulation of one neuron increased SIC frequency in adjacent MSNs (n = 12 D1-D1 and 15 D2-D2 pairs). In contrast, in heterotypic pairs, MSN stimulation failed to increase the SIC frequency (n = 17 D1-D2 and 13 D2-D1 pairs, where D1 or D2 MSNs were stimulated and SICs were recorded from D2 or D1 MSNs, respectively) (Fig. 3, H and I). This indicates that the nonsynaptic astrocyte-mediated communication between MSNs was specific of homotypic cell subtypes and restricted to particular striatal pathways. These results suggest the existence of functional astro-neuronal networks defined by the presence of selective astrocyte-neuron bidirectional signaling between specific cell subtypes.

We therefore asked whether subpopulations of astrocytes regulated specific subsets of synapses belonging to the direct and indirect basal ganglia pathways. We performed triple whole-cell recordings of sets of two heterotypic MSNs with a single astrocyte. We first identified astrocytes that responded to the depolarization of either D1 or D2 MSNs. Then, an identified astrocyte was loaded with NP-EGTA (5 mM) to be stimulated by UV-flash photolysis. Finally, another pair of heterotypic neurons was recorded to monitor the synaptic responses (Fig. 4, A to C). Uncaging of Ca^{2+} in astrocytes that responded to D1-MSN stimulation evoked a transient synaptic potentiation exclusively in D1 MSNs (n = 7 out of 9 triple recordings) without affecting neurotransmission in D2 MSNs (n = 9 out of 9 triple recordings). Likewise, selective UV-flash stimulation of D2-responding astrocytes selectively enhanced synaptic transmission in D2 (n = 8 out of 9) but not in D1 MSNs (n = 9 out of 9) (Fig. 4, D and E). These results indicate that astrocyte-mediated synaptic regulation is restricted to signaling between subsets of astrocytes and particular synapses.

Although some reports have questioned the physiological significance of the astrocyte Ca^{2+} signal and its neuromodulatory consequences (7, 8), our findings reveal that this signal can be triggered by endogenous stimuli of neuronal origin and that its effects on synaptic function are delicately regulated.

Astrocytes and neurons in the dorsal striatum selectively interact in a cell- and synapse-specific manner, and striatal astrocytes display a functional

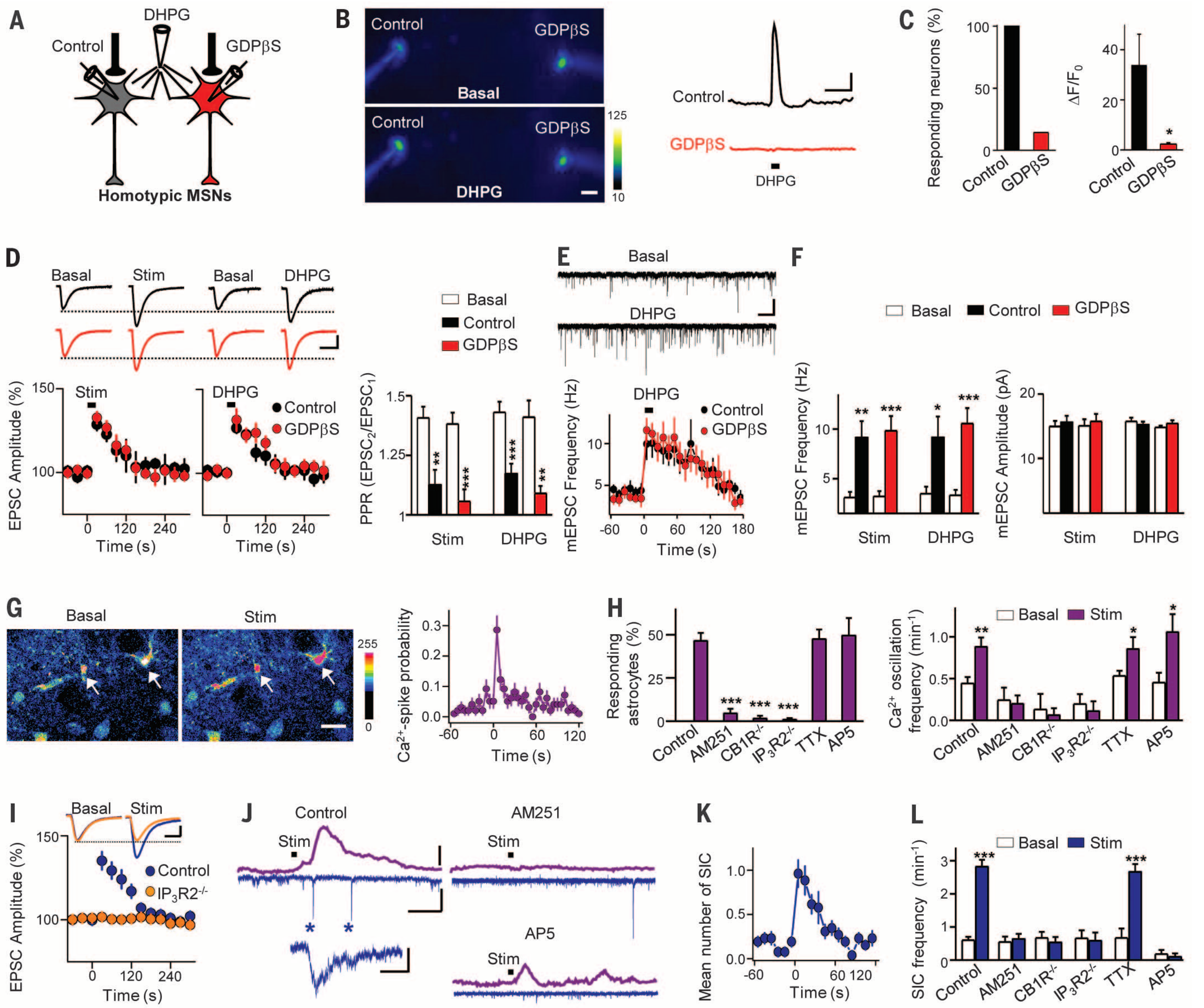

Fig. 2. Bidirectional astrocyte-neuron signaling regulates MSN excitability and synaptic transmission. (**A**) Scheme showing homotypic MSN pair recordings. One neuron was loaded with GDP-β-S. (**B**) Pseudocolor images of homotypic MSNs loaded with fluo-4 (control) and fluo-4 and GDP-β-S before (basal) and after local application of DHPG (scale bar, 20 μm). Colors correspond to fluorescence levels. MSN Ca^{2+} responses are shown to the right [scale bars, 20% (vertical) and 20 s (horizontal)], with the application of DHPG indicated by the black bar. (**C**) Responding neurons and increases in fluorescence evoked by DHPG in control and GDP-β-S–loaded MSNs (n = 7 MSN pairs). (**D**) EPSCs before and after homotypic MSN stimulation and DHPG application (top). The bottom left panel shows relative EPSC amplitudes over time. The bottom right panel shows PPR before and after stimulation and DHPG application in control (n = 8 stim and 8 DHPG) and GDP-β-S–loaded (n = 10 stim and 11 DHPG) neurons. The scale bars are 25 pA (vertical) and 15 ms (horizontal). (**E**) MSN whole-cell currents showing mEPSCs before and after DHPG application (top), with mean mEPSC frequency over time before and after DHPG application (black bar) in control (n = 8) and GDP-β-S–loaded (n = 8) neurons (bottom). The scale bars are 25 pA (vertical) and 5 s (horizontal). (**F**) mEPSC frequency and amplitude 1 min before and after stimulation and DHPG application in control and GDP-β-S–loaded neurons (each bar: n ≥ 8 MSN pairs). (**G**) Pseudocolor images of fluo-4–filled astrocytes (indicated by arrows) before and after MSN stimulation, with astrocyte Ca^{2+}-spike probability shown to the right. The scale bar is 10 μm. (**H**) The proportion of astrocytes that responded to neuronal stimulation (left) and Ca^{2+} oscillation frequency (right) before and after stimulation in control and various experimental configurations (each bar: n ≥ 71 astrocytes, n ≥ 9 slices). (**I**) EPSCs before and after stimulation in control (n = 8 MSN pairs, 8 slices) and $IP_3R2^{-/-}$ (n = 28 MSN pairs, 28 slices) mice, with relative EPSC amplitude changes. The scale bars are 25 pA (vertical) and 15 ms (horizontal). (**J**) Representative astrocyte Ca^{2+} levels (purple; scale bar, 20%) and MSN whole-cell currents [blue; scale bars, 25 pA (vertical) and 30 s (horizontal)] in control, AM251, and AP5. Black bars indicate stimulation. Asterisks indicate SICs. The insert shows an expanded SIC [scale bars, 25 pA (vertical) and 250 ms (horizontal)]. (**K**) Mean number of SICs over time. (**L**) Mean SIC frequency before and after stimulation in different experimental configurations (each bar: n ≥ 8 MSN pairs). *P < 0.05, **P < 0.01, ***P < 0.001; Student's t test. Data are expressed as mean ± SEM.

heterogeneity based on selective signaling with particular neuron subtypes and synapses belonging to the basal ganglia's direct and indirect pathways (Fig. 4F). The activities of both pathways are fundamental in motor control (*27*), and their imbalances underlie motor deficits in Parkinson's (*10*, *11*, *28*, *29*) and Huntington's diseases (*30*). Selective regulation of specific synapses by astrocytes indicates that they may be involved in the

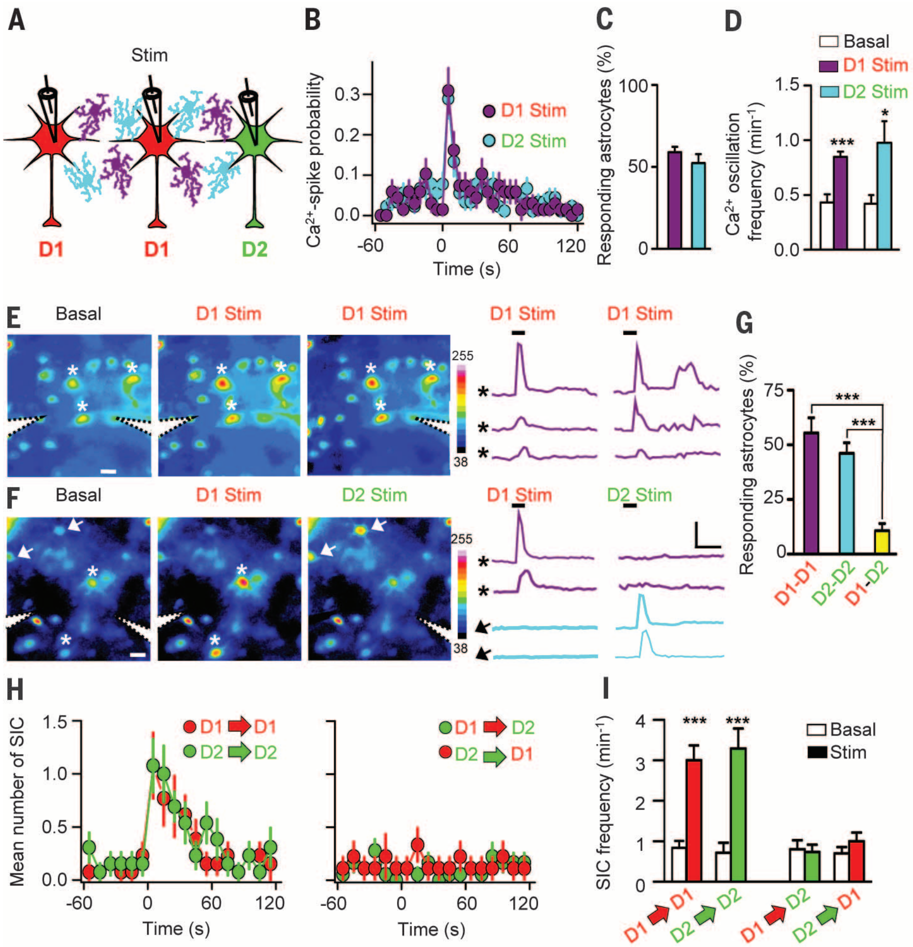

Fig. 3. Astrocyte-neuron signaling is cell type–specific. (**A**) Scheme showing stimulation of one MSN and synaptic currents recorded in homotypic or heterotypic MSNs while monitoring astrocyte Ca^{2+} levels (purple, D1-MSN-responding astrocytes; blue, D2-MSN–responding astrocytes). (**B**) Ca^{2+}-spike probability for astrocytes, (**C**) proportion of responding astrocytes, and (**D**) Ca^{2+} oscillation frequency for astrocytes before (basal) and after stimulation of D1 or D2 MSNs (each bar: $n \geq 235$ astrocytes, $n \geq 26$ slices; $^*P < 0.05$, $^{***}P < 0.001$; Student´s *t* test). (**E**) Pseudocolor images (left) of astrocytes (indicated by asterisks; scale bar, 10 μm) and corresponding Ca^{2+} responses (right) before and after consecutive stimulation of a homotypic D1 MSN pair. On the left, colors correspond to fluorescence levels. On the right, horizontal bars indicate neuronal stimulation [vertical and horizontal scales follow (F)]. (**F**) As in (E), but stimulating a heterotypic MSN pair. Asterisks and arrows indicate astrocytes responding to D1- and D2-MSN stimulation, respectively. The scale bars are 20% (vertical) and 10 s (horizontal). (**G**) Percentage of astrocytes responding to consecutive stimulation of homotypic and heterotypic MSNs (each bar: $n \geq 117$ astrocytes, $n \geq 12$ slices; $^{***}P < 0.001$; Fisher´s test). (**H**) Mean number of SICs before and after D1- or D2-MSN stimulation, recorded in homotypic and heterotypic adjacent MSNs. (**I**) Mean SIC frequency recorded in D1 and D2 MSNs before and after neuronal stimulation of homotypic and heterotypic MSNs (each bar: $n \geq 12$ MSN pairs from $n \geq 12$ slices; $^{***}P < 0.001$; Student´s *t* test). Data are expressed as mean ± SEM.

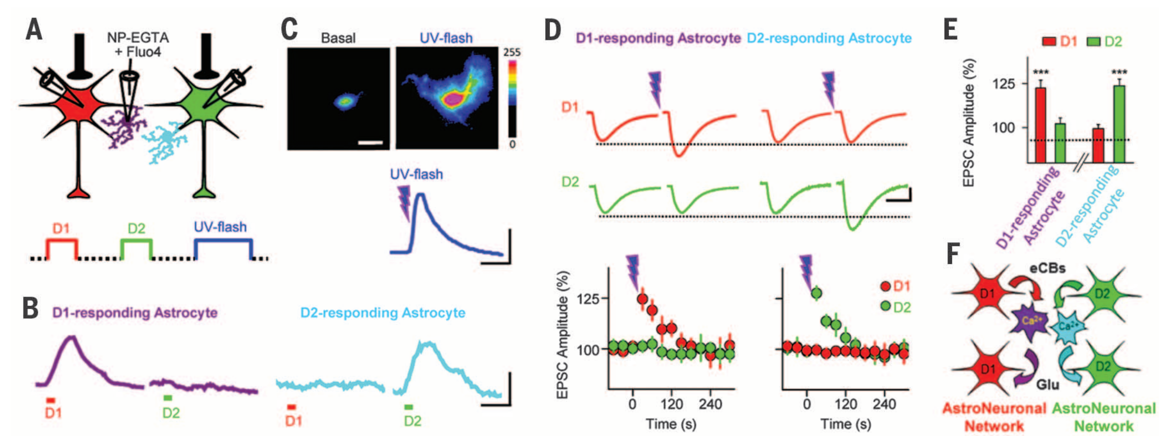

Fig. 4. Synapse-specific regulation of striatal transmission by selective stimulation of particular astrocytes. (**A**) Scheme depicting triple recordings of two heterotypic MSNs and one NP-EGTA– and fluo-4–filled astrocyte (top); the D1- and D2-MSN stimulation protocol for identifying responding astrocytes (consecutive depolarization of D1 and D2 MSNs) and for UV-flash astrocyte stimulation (bottom). (**B**) Intracellular Ca^{2+} levels of two single astrocytes selectively responding to D1- or D2-MSN stimulation. The scale bars are 10% (vertical) and 20 s (horizontal). (**C**) Pseudocolor images of a fluo-4–filled astrocyte before (basal) and after UV-flash stimulation (top; scale bar, 10 μm) and corresponding Ca^{2+} levels [bottom; scale bars, 10% (vertical) and 20 s (horizontal)]. Colors correspond to fluorescence levels. (**D**) Averaged EPSCs [top; scale bars, 25 pA (vertical) and 15 ms (horizontal)], EPSC amplitude changes (bottom), and (**E**) relative EPSC amplitude changes recorded from D1 and D2 MSNs before and after UV-flash stimulation of D1- or D2-responding astrocytes ($n = 9$ and 9; $^*P < 0.05$, $^{***}P < 0.001$; Student´s *t* test). Data are expressed as mean ± SEM. (**F**) Scheme representing striatal astro-neuronal networks. Stimulation of MSNs (D1 or D2) promotes eCB release that increases Ca^{2+} in a specific subpopulation of astrocytes, which then release glutamate that modulates excitability and synaptic transmission selectively in homotypic neurons through activation of NMDARs and group I mGluRs, respectively.

coordinated activity of these networks in the striatal function, and, therefore, they may participate in its dysfunction in brain disorders. Our results demonstrate the existence of functional astro-neuronal networks that comprise subpopulations of astrocytes, neurons, and synapses belonging to specific brain circuits, which may differentially control specific circuit activity through selective signaling between particular astrocytes and neurons.

REFERENCES AND NOTES

1. A. Araque *et al.*, *Neuron* **81**, 728–739 (2014).
2. C. Eroglu, B. A. Barres, *Nature* **468**, 223–231 (2010).
3. M. M. Halassa, P. G. Haydon, *Annu. Rev. Physiol.* **72**, 335–355 (2010).
4. G. Perea, M. Navarrete, A. Araque, *Trends Neurosci.* **32**, 421–431 (2009).
5. A. Volterra, J. Meldolesi, *Nat. Rev. Neurosci.* **6**, 626–640 (2005).
6. G. Perea, A. Araque, *Science* **317**, 1083–1086 (2007).
7. C. Agulhon, T. A. Fiacco, K. D. McCarthy, *Science* **327**, 1250–1254 (2010).
8. T. A. Fiacco *et al.*, *Neuron* **54**, 611–626 (2007).
9. B. C. Shonesy *et al.*, *Nat. Neurosci.* **16**, 456–463 (2013).
10. A. C. Kreitzer, R. C. Malenka, *Nature* **445**, 643–647 (2007).
11. W. Shen, M. Flajolet, P. Greengard, D. J. Surmeier, *Science* **321**, 848–851 (2008).
12. M. Uchigashima *et al.*, *J. Neurosci.* **27**, 3663–3676 (2007).
13. V. Chevaleyre, K. A. Takahashi, P. E. Castillo, *Annu. Rev. Neurosci.* **29**, 37–76 (2006).
14. A. C. Kreitzer, R. C. Malenka, *Neuron* **60**, 543–554 (2008).
15. R. L. Albin, A. B. Young, J. B. Penney, *Trends Neurosci.* **12**, 366–375 (1989).
16. L. M. Suárez *et al.*, *Biol. Psychiatry* **75**, 711–722 (2014).
17. S. Ares-Santos, N. Granado, I. Espadas, R. Martinez-Murillo, R. Moratalla, *Neuropsychopharmacology* **39**, 1066–1080 (2014).
18. M. Gómez-Gonzalo *et al.*, *Cereb. Cortex* (2014).
19. M. Navarrete, A. Araque, *Neuron* **68**, 113–126 (2010).
20. R. Min, T. Nevian, *Nat. Neurosci.* **15**, 746–753 (2012).
21. M. Navarrete *et al.*, *PLOS Biol.* **10**, e1001259 (2012).
22. M. A. Di Castro *et al.*, *Nat. Neurosci.* **14**, 1276–1284 (2011).
23. J. Petravicz, T. A. Fiacco, K. D. McCarthy, *J. Neurosci.* **28**, 4967–4973 (2008).
24. T. Fellin *et al.*, *Neuron* **43**, 729–743 (2004).
25. M. Navarrete, A. Araque, *Neuron* **57**, 883–893 (2008).
26. G. Perea, A. Araque, *J. Neurosci.* **25**, 2192–2203 (2005).
27. G. Cui *et al.*, *Nature* **494**, 238–242 (2013).
28. A. V. Kravitz *et al.*, *Nature* **466**, 622–626 (2010).
29. I. Ruiz-DeDiego, B. Mellstrom, M. Vallejo, J. R. Naranjo, R. Moratalla, *Biol. Psychiatry* **77**, 95–105 (2015).
30. V. M. André *et al.*, *J. Neurosci.* **31**, 1170–1182 (2011).

ACKNOWLEDGMENTS

We thank D. Redish, W. Buño, A. Díez, and R. Gómez for helpful comments; J. Lerma and A. Valero for valuable help; B. Pro for technical assistance; and J. Chen (University of California–San Diego) and A. Zimmer (University of Bonn) for providing $IP_3R2^{-/-}$ and $CB1R^{-/-}$ mice, respectively. A.A. was supported by Cajal Blue Brain, the Human Frontier Science Program (grant RGP0036/2014), the Wallin family, and V. and L. Han. Support for this work was also provided by the Ministerio de Economía y Competitividad of Spain (grants BFU2013-47265-R, CSD2010-00045, and RYC-2012-12014 to G.P. and grants SAF2013-48532-R and CB06/05/0055 to R.Mo.) and by the Juan de la Cierva Program (grant JCI-2010-07693 to R.Ma.). Data described in the paper are archived at the Instituto Cajal (Madrid, Spain). The authors declare no competing financial interests.

SUPPLEMENTARY MATERIALS

www.sciencemag.org/content/349/6249/730/suppl/DC1
Materials and Methods
Figs. S1 to S7
References (*31*–*39*)

28 January 2015; accepted 17 June 2015
10.1126/science.aaa7945

LANGUAGE DEVELOPMENT

The developmental dynamics of marmoset monkey vocal production

D. Y. Takahashi,[1,2]* A. R. Fenley,[1,2] Y. Teramoto,[1] D. Z. Narayanan,[1,2] J. I. Borjon,[1,2] P. Holmes,[1,3] A. A. Ghazanfar[1,2,4]*

Human vocal development occurs through two parallel interactive processes that transform infant cries into more mature vocalizations, such as cooing sounds and babbling. First, natural categories of sounds change as the vocal apparatus matures. Second, parental vocal feedback sensitizes infants to certain features of those sounds, and the sounds are modified accordingly. Paradoxically, our closest living ancestors, nonhuman primates, are thought to undergo few or no production-related acoustic changes during development, and any such changes are thought to be impervious to social feedback. Using early and dense sampling, quantitative tracking of acoustic changes, and biomechanical modeling, we showed that vocalizations in infant marmoset monkeys undergo dramatic changes that cannot be solely attributed to simple consequences of growth. Using parental interaction experiments, we found that contingent parental feedback influences the rate of vocal development. These findings overturn decades-old ideas about primate vocalizations and show that marmoset monkeys are a compelling model system for early vocal development in humans.

Human vocal development is the outcome of interactions among an infant's developing body and nervous system and his or her experience with caregivers (*1*, *2*). Infant cries decline over the first 3 months as they transition into preverbal vocalizations (*3*). The rates of these transitions are influenced by social feedback: Contingent responses of caregivers spur the development of more mature vocalizations (*4*). In contrast, nonhuman primate vocalizations are widely viewed as undergoing little or no production-related acoustic changes during development, and any such changes are attributed solely to passive consequences of growth (*5*).

We tracked the vocal development of marmoset monkeys (*Callithrix jacchus*; $n = 10$)—a voluble, cooperative breeding species (*6*)—from the first postnatal day (P1) until they produced adultlike calls at 2 months of age. Recordings were taken at least twice weekly in two contexts: undirected (social isolation) and directed (with auditory, but not visual, contact with their mother or father). Such early and dense sampling is necessary to accurately capture developmental changes in marmosets because this species develops rapidly (*7*). Each recording session began with ~5 min in the undirected context followed by ~15 min in the directed context, with mothers and fathers alternating between each session. In the undirected context, infants exhibited a dramatic change in vocal production (Fig. 1A and audio S1 to S8). At P1, vocalizations were more numerous and variable in their spectrotemporal structure than those recorded in later weeks. The number and variability of calls diminished over 2 months, approaching mature vocal output with exclusive production of whistle-like "phee" calls in this context (*8*).

To quantify this developmental change as a continuous process without the bias of ethological labels (*9*), for each of the 73,421 recorded utterances, we measured four acoustic parameters similar to those used for tracking birdsong development (*10*): duration, dominant frequency, amplitude modulation (AM) frequency, and Wiener entropy (a measure of spectral flatness) (Fig. 1B). Changes in all four parameters were statistically significant ($n = 301$ sessions, $P < 0.001$), showing that vocalizations underwent a transformation in the first 2 months, whereby utterances lengthened, dominant and AM frequencies decreased, and entropy decreased. This pattern of change is consistent with both human and songbird vocal development (*10*, *11*). These changes in infant vocalizations, although not subtle, may be due solely to physical maturation (*5*). To test this, we used body weight as a proxy for overall growth [weight correlates well with vocal apparatus size in monkeys (*12*)]. Weight changes visibly contrasted with the trajectories of the acoustic parameters (Fig. 1, B and C). To quantify this difference, we used weight to predict changes in the acoustic parameters. Predicted average parameter values, given the average weight for each postnatal day, are shown in Fig. 1B. If growth completely explained the acoustic change, the residues would be uncorrelated and identically distributed across postnatal days. Using the Akaike information criterion (AIC), the best polynomial-fit order was three

[1]Princeton Neuroscience Institute, Princeton University, Princeton, NJ 08544, USA. [2]Department of Psychology, Princeton University, Princeton, NJ 08544, USA. [3]Department of Mechanical and Aerospace Engineering and Program in Applied and Computational Mathematics, Princeton University, Princeton, NJ 08544, USA. [4]Department of Ecology and Evolutionary Biology, Princeton University, Princeton, NJ 08544, USA.
***Corresponding author. E-mail: takahashiyd@gmail.com (D.Y.T.); asifg@princeton.edu (A.A.G.)**

Science AAAS

Circuit-specific signaling in astrocyte-neuron networks in basal ganglia pathways
R. Martín *et al.*
Science **349**, 730 (2015);
DOI: 10.1126/science.aaa7945